AIAA JOURNAL
Vol. 31, No. 10, October 1993

Shock-Wave Reflection over a Semicircular Cylinder in a Dusty Gas

Xiaolong Yang,* Shmuel Eidelman,† and Itzhak Lottati*
Science Applications International Corporation, McLean, Virginia 22102

The unsteady shock-wave reflection and diffraction generated by a shock wave propagating over a semicircular cylinder in a dusty gas are studied numerically. The mathematical model is a multiphase system based on a multifluid Eulerian approach. A second-order Godunov scheme is used to solve the gas-phase Euler equations and an upwind scheme is used to solve the particle-phase conservation equations on an unstructured adaptive mesh. For the validation of the model, the numerically predicted one-dimensional shock-wave attenuation is compared with experimental results. Shock-wave reflection and diffraction over a semicircular cylinder in a pure gas flow is simulated first to show the excellent agreement between the present computation and the experimental results. For a shock-wave reflection and diffraction in a dusty gas, the effects of particle size and particle loading on the flowfield are investigated. Gas and particle-density contour plots are presented. It has been shown that the shock-wave configuration differs remarkably from pure gas flow depending on the particle parameters. The difference is explained as the result of momentum and heat exchange between the two phases.

I. Introduction

SHOCK-WAVE propagation into a gas-particle-suspension medium has attracted great attention in recent years due to its many engineering applications. Some of these applications include blast wave propagating over a dusty surface, exhaust from a solid-propellant rocket, and coal or grain dust detonation. Many studies dealing with two-phase environment can be found in the literature. A general description and theoretical analysis of such flow can be found in review papers by Marble[1] and by Rudinger,[2] and in a book by Soo.[3] Numerical models for dilute gas-particle flows were reviewed by Crowe.[4] Numerical studies of gas-particle flow in a solid rocket nozzle can be found in Refs. 5 and 6. Miura and Glass[7] theoretically and numerically studied the oblique shock waves in a dusty-gas flow over a wedge. The one-dimensional unsteady structure of shock waves propagating through a gas-particle mixture was investigated both experimentally and numerically by Sommerfeld.[8] Recently, Kim and Chang[9] illustrated a numerical simulation of shock-wave propagation into a dusty gas and the reflection of the wave from a wedge. Shock-wave ignition of different reactive dust is experimentally investigated by Sichel et al.[10] and the comprehensive model for the structure of dust detonations is also described by Fan and Sichel.[11]

In this paper, we study shock-wave reflection and diffraction over a semicircular cylinder in a dusty gas. We numerically simulate the problem of a shock wave initiated in a pure gas section moving into a dusty region and impinging on a semicircular cylinder. We first formulate the compressible two-phase flow on the basis of a Eulerian multifluid formulation. We consider the two phases (i.e., gas and particle) to be interpenetrating continua. The dynamics of the flow are governed by conservation equations of each phase and the two phases are coupled by interactive drag force and heat transfer. We solve the system of conservation equations numerically on an unstructured adaptive grid. The objectives of the study are 1) to solve the two-phase compressible flowfield and compare the simulation with available experimental results; and 2) to observe and investigate the reflection and diffraction wave patterns when a shock wave propagates over a semicircular cylinder in a dusty gas, with particle radius and loading as parameters.

The outline of this paper is as follows. Section II gives a description of the mathematical model and method of numerical solution, including governing conservation equations for two phases, the constitutive laws, the initial and boundary conditions, and particle parameter. A brief outline of numerical schemes and the adaptive unstructured grid is also given. In Sec. III, we present our numerical simulation results. We validate our model by comparing a one-dimensional simulation of a shock wave propagating into a dusty gas with available experimental results. We also show the excellent agreement between our two-dimensional gas-only simulation with existing experimental results. Results for reflection and diffraction of shock wave over a semicircular cylinder are given for different particle parameters. Concluding remarks are given in Sec. IV.

II. Mathematical Model and Numerical Solution

Conservation Equations

The mathematical model consists of conservation governing equations and constitutive laws that provide closure for the model. The basic formulation adopted here follows the gas and dilute particle flow-dynamics model presented by Soo.[3] The following assumptions are used during the derivation of governing equations:

1) The gas is air and is assumed to be ideal gas.
2) The particles do not undergo a phase change because for particles considered here (sand) phase transition temperature is much higher than the temperatures typical for the simulated cases.
3) The particles are solid spheres of uniform diameter and have a constant material density.
4) The volume occupied by the particles is negligible.
5) The interaction between particles can be ignored.
6) The only force acting on the particles is drag force and the only heat transfer between the two phases is convection. The weight of the solid particles and their buoyancy force are negligibly small compared to the drag force.
7) The particles have a constant specific heat and are assumed to have a uniform temperature distribution inside each particle.

Under the above assumptions, distinct equations of continuity, momentum, and energy are written for each phase. The interaction effects between the two phases are listed as the source terms on the right-hand side of the governing equation.

Received Aug. 18, 1992; revision received Feb. 23, 1993; accepted for publication Feb. 23, 1993.

*Research Scientist, 1710 Goodridge Drive, MS 2-3-1.
†Research Scientist, 1710 Goodridge Drive, MS 2-3-1. Associate Fellow AIAA.

The two-dimensional unsteady conservation equations for the two phases can be written in the vector form in Cartesian coordinates:

$$\frac{\partial U}{\partial t}+\frac{\partial F}{\partial x}+\frac{\partial G}{\partial y}=S \tag{1}$$

Here U is the vector of conservative variables, F and G are fluxes in the x and y directions, respectively, and S is the source term for momentum and heat exchange. The definitions of these vectors are

$$U=\begin{vmatrix}\rho\\ \rho u\\ \rho v\\ e\\ \rho_p\\ \rho_p u_p\\ \rho_p v_p\\ e_p\end{vmatrix},\quad F=\begin{vmatrix}\rho u\\ \rho u^2+p\\ \rho uv\\ u(e+p)\\ \rho_p u_p\\ \rho_p u_p^2\\ \rho_p u_p v_p\\ u e_p\end{vmatrix}$$

$$G=\begin{vmatrix}\rho v\\ \rho uv\\ \rho v^2+p\\ v(e+p)\\ \rho_p u_p\\ \rho_p u_p v_p\\ \rho_p v^2 p\\ v_p e_p\end{vmatrix},\quad S=\begin{vmatrix}0\\ -f_x\\ -f_y\\ -q-u_p f_x-v_p f_y\\ 0\\ f_x\\ f_y\\ q+u_p f_x+v_p f_y\end{vmatrix}$$

where ρ, u, v, and e are gas density, velocities, and energy, respectively; ρ_p, u_p, v_p, and e_p are particle density, velocities, and energy, respectively; and (f_x, f_y) and q denote drag force components acting on the particles and heat transfer to the particles, respectively. The gas pressure p is related to ρ, u, v, and e by

$$p=(\gamma-1)[e-0.5\rho(u^2+v^2)] \tag{2}$$

where γ is the specific heat ratio. The gas temperature can be found through the equation-of-state for ideal gas:

$$p=\rho RT \tag{3}$$

where R is the gas constant. The particle temperature T_p is calculated through the relation

$$e_p=\rho_p c_p T_p+0.5\rho_p(u_p^2+v_p^2) \tag{4}$$

The source terms on the right-hand side of Eq. (1) are momentum and heat exchange between gas and particle phases. If we let r_p and ρ_s be the particle radius and material density, respectively, then the drag forces are

$$\begin{pmatrix}f_x\\ f_y\end{pmatrix}=\frac{3}{8}\left(\frac{\rho_p\rho}{\rho_s r_p}\right)C_d\,[(u-u_p)^2+(v-v_p)^2]^{1/2}\begin{bmatrix}(u-u_p)\\ (v-v_p)\end{bmatrix} \tag{5}$$

The particle drag coefficient C_d depends on relative Reynolds number Re and relative Mach number M_r. In the present study, since the relative Mach number is small ($M_r<0.5$), the effect of M_r on C_d is neglected. The Reynolds number Re is based on the relative velocity between the gas and particle phases. After testing the drag coefficients given by Sommerfeld[8] and by Clift et al.,[12] the following two were adopted:

$$C_d=24/Re\,(1+0.15Re^{0.687}) \qquad \text{for} \quad Re<800 \tag{6a}$$

$$C_d=24/Re\,(1+0.15Re^{0.687})+0.42/(1+42{,}500Re^{-1.16}) \qquad \text{for} \quad Re>800 \tag{6b}$$

Here the Reynolds number Re is defined as

$$Re=\frac{2\rho r_p[(u-u_p)^2+(v-v_p)^2]^{1/2}}{\mu} \tag{7}$$

Viscosity μ is calculated at film temperature, namely, $T_f=0.5\,(T_p+T)$, and the temperature dependency of the viscosity is evaluated according to Sutherland's law

$$\mu=\mu_r\,(T/T_r)^{3/2}(T_r+\Phi)/(T+\Phi) \tag{8}$$

where μ_r is the dynamic viscosity of the gaseous phase at the reference temperature and Φ is an effective temperature, called the Sutherland constant.

The rate of heat transfer from gaseous phase to the particle phase is given by

$$Q=(3/2)(\rho_p/\rho_s)(\mu C_p/Pr)Nu(T-T_p) \tag{9}$$

where $Pr=\mu c_p/k_g$ is the Prandtl number, and c_p and k_g are the specific heat and thermal conductivity of gas, respectively. The Nusselt number Nu is a function of Reynolds number and the Prandtl number as given by Drake[13]:

$$Nu=2r_p h/\mathrm{kg}=2+0.459Re^{0.55}Pr^{0.33} \tag{10}$$

Initial and Boundary Conditions

The geometry of the computational domain is shown in Fig. 1. The initial conditions for gas are $\rho_o=1.2$ kg/m^3 and $p_o=101.3$ kPa, with a coming shock at $x=-0.5$. There are no particles from $-1.0\le x\le 0.0$. From $x\ge 0.0$, particles are initially in thermal and kinematic equilibrium with the surrounding gas. The particles that are uniformly distributed in the dusty region have the following parameters for different test problems:

Mass loading ρ_p:	0.25 and 0.76 kg/m^3;
Mass material density ρ_s:	2500 kg/m^3;
Particle radii r_p:	10, 25, and 50 μm;
Specific heat c_s:	766 J/kg/K

The lower boundary and cylinder surface are solid walls and assumed adiabatic and impermeable. A reflecting boundary condition is assumed for both the gas and particle phase. Particles are assumed to experience a perfect elastic collision with the wall and reflect from the wall. The right and upper boundaries are open boundaries where a nonreflection

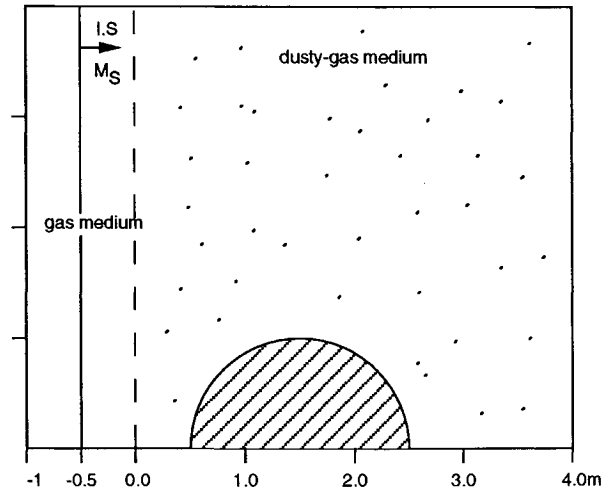

Fig. 1 Illustration of the considered flowfield.

boundary condition is used for the gas phase and a zero normal gradient condition is used for particle phase.

Numerical Method of Solutions

The system of partial differential equations described in the previous paragraph is integrated numerically. Equation (1) is repeated here:

$$\frac{\partial U}{\partial t}+\frac{\partial F}{\partial x}+\frac{\partial G}{\partial y}=S$$

To solve this equation numerically, an operator time-splitting technique is used. Assuming that all flow variables are known at a given time, we can calculate its advancement in time by splitting the integration into two stages.

In the first stage, the conservative part of Eq. (1) is solved:

$$\frac{\partial U}{\partial t}+\frac{\partial F}{\partial x}+\frac{\partial G}{\partial y}=0 \tag{11}$$

The second-order Godunov method is used for the integration of the subsystem of equations describing the flow of the gaseous phase [first four components of Eq. (1)]. The method is well documented in the literature.[14-16] The subsystem of equations describing the particle-phase flow is integrated using a simple first-order finite difference upwind scheme.[17] This is done because there is no shock in the particle phase and the upwind scheme leads to a robust and accurate integration scheme.

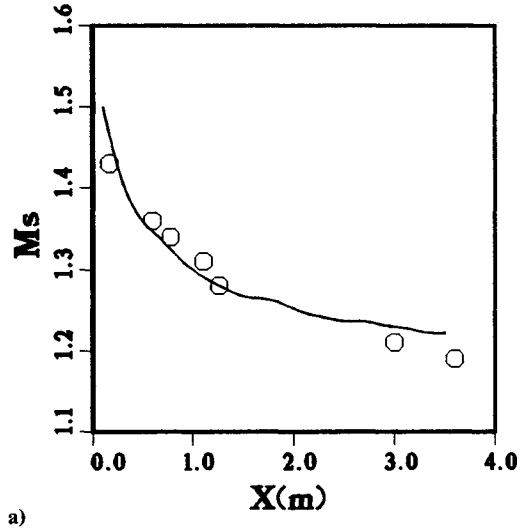

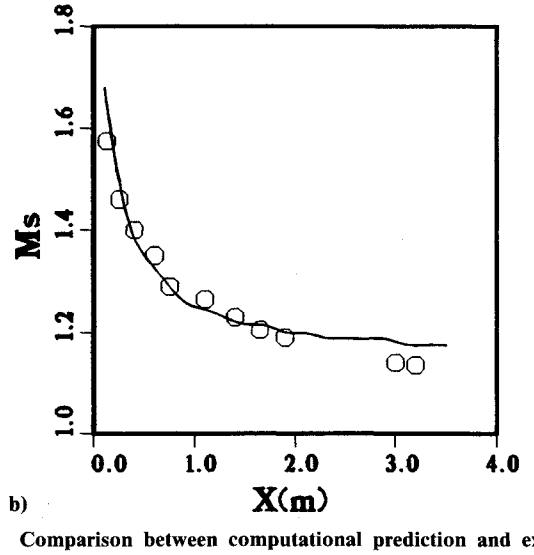

Fig. 2 Comparison between computational prediction and experimental measurement of shock-wave attenuation: a) $M_s = 1.49$, $\eta = \rho_p/\rho_o = 0.63$ and b) $M_s = 1.7$, $\eta = \rho_p/\rho_o = 1.4$ (o : experiment, ——: calculation).

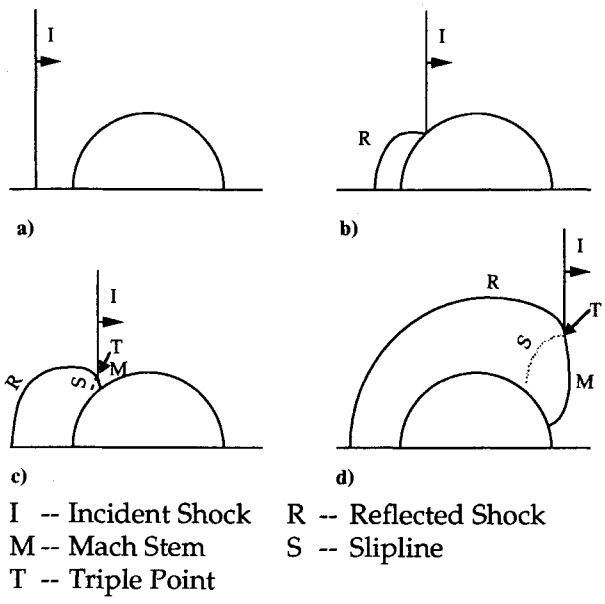

Fig. 3 Stages of shock-wave reflection over a semicircular cylinder: a) before collision; b) regular reflection; c) Mach reflection; and d) well-developed Mach reflection.

In the second stage, the source term is added and the following equation is solved:

$$\frac{\partial U}{\partial t}=S \tag{12}$$

To integrate this equation in time, we need to obtain S as a function of U. We calculate S through Eqs. (5-10).

To produce a solution of the high spatial accuracy at minimal computational cost, an unstructured triangular grid with adaptive procedure is used. The adaptive procedure will automatically enrich the mesh by adding points in the high gradient (or high flow activity) region of the flowfield and by removing points (coarsening mesh) where they are not needed. The dynamic nature of mesh enrichment is shown in Fig. 4 for three different time frames. One can see that a very fine mesh is generated around shock fronts and other steep density gradient regions.

III. Results

Model Validation for One-Dimensional Shock Wave Propagation in Dusty Gas

To test the momentum and heat exchange mechanism for the current two-phase model, we first simulate a one-dimensional problem of a normal shock wave propagating into a dusty gas. We numerically simulate the experiments conducted by Sommerfeld.[8] In the experiments, small glass spherical particles of material density $\rho_s = 2500$ kg/m^3, specific heat capacity $c_s = 766$ J/kg/K, and average diameter of 27 μm were used as the suspension particle phase. The incoming shock Mach number M_s and particle loading ratio $\eta = \rho_p/\rho$, are two varying parameters. The experimental results and our numerical simulation results of shock Mach number as a function of distance for two test cases are shown in Fig. 2a ($\eta = 0.63$, $M_s = 1.49$) and Fig. 2b ($\eta = 1.4$, $M_s = 1.7$) for comparison purposes. It is clear that the agreement between the prediction of shock-wave attenuations from our present model and the experimental results is very good.

Two-Dimensional Simulation Results for Pure Gas Flow

To test the accuracy of the two-dimensional computation, we first compute the pure gas-flow case of a shock-wave

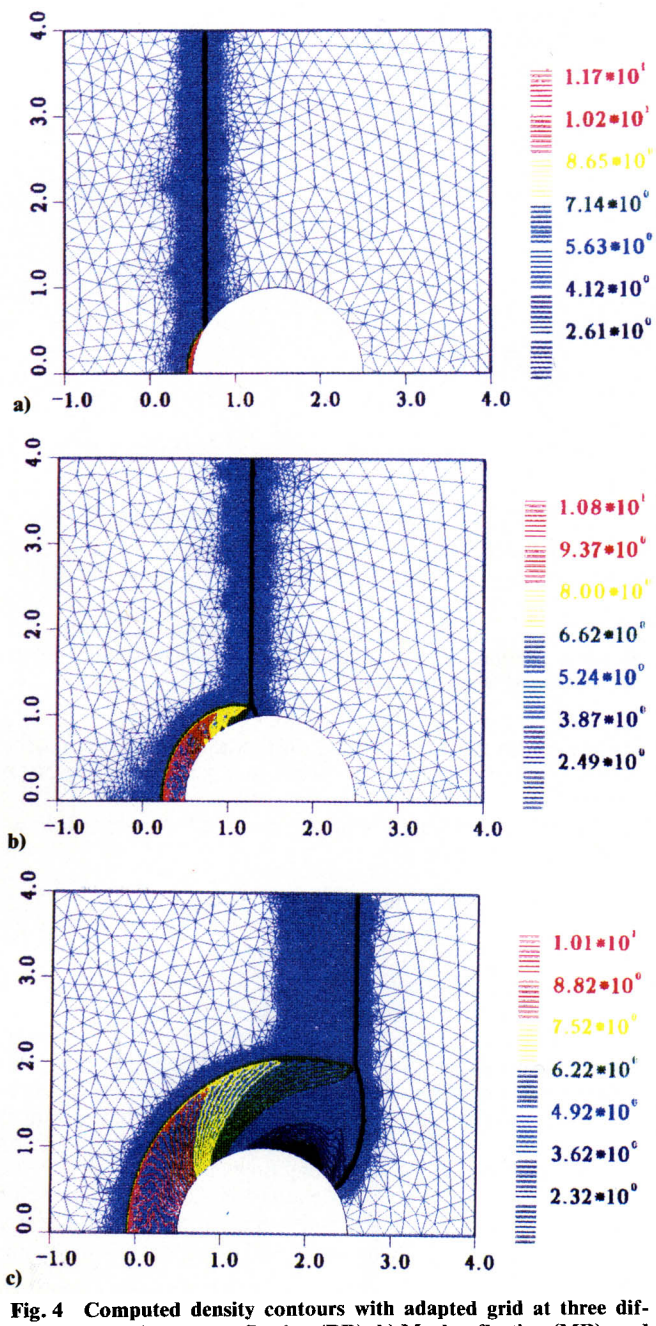

Fig. 4 Computed density contours with adapted grid at three different times: a) regular reflection (RR); b) Mach reflection (MR); and c) diffraction with slipline (S).

reflection and diffraction over a semicircular cylinder. We then compare the simulation with experimental results. Shock-wave reflection on a wedge has been extensively studied by many researchers (see e.g., review papers of Ben-Dor and Dewey[18] and Hornung[19]). Shock-wave reflection over circular cylinders was numerically simulated by Yang et al.[20] Recently, Glass et al.,[21] using the high-order Godunov scheme, numerically simulated the shock-wave reflection over a half-diamond and semicircular cylinder and compared the simulation with experimental results obtained by Kaca.[22] Figure 3 is a schematic sketch to show four stages of a shock-wave reflection over a semicircular cylinder and terminologies which will be used to describe the flowfields. Figures 4a–4c show the calculated density contours at three moments in time. When the planar shock wave propagates and encounters the cylinder, it first experiences a head-on collision with the front stagnation point of the semicylinder and then immediately reflects from the first quarter of the cylinder, forming a regular reflection (RR), which is shown in Fig. 4a. The regular reflection consists of two shocks, i.e., the incident shock and reflected shock, both originating from a common point on the cylinder wall. As the shock wave propagates up the cylinder, the angle between the incident shock and the tangent of the cylinder becomes larger and the regular reflection changes into a Mach reflection (MR) as shown in Fig. 4b. The MR is characterized by three waves, incident shock (I), reflected shock (R), and Mach stem (M). All three shocks intersect at one common point called triple point (T). For Mach reflection, one can further observe both simple Mach reflection (SMR) and complex Mach reflection (CMR). Later, as the incident shock-wave passes over the top of the semicircular cylinder, it experiences a rarefaction on the back side of the cylinder. The shock wave system grows upward and rightward with a curved Mach stem and forms a slipline (S) or a contact discontinuity (CD) as shown in Fig. 4c. In Figs. 5a and 5b, the interferogram from the experiment[22] and density contours from the present simulation are compared for the same flow condition and same time. Note that the density levels are normalized by the ambient gas density in Fig. 5. As one can see from Fig. 5, the results show an excellent quantitative as well as qualitative agreement between the numerical simulation and experimental results.

Two-Dimensional Simulation Results of Two-Phase Flow

The basic setup for the two-phase simulation is shown in Fig. 1. Here the planar shock with $M_s = 2.8$ propagates into an area of a dusty gas and impinges on a semicircular cylinder. The interface between pure air and dusty air is located at $x = 0.0$ of the computational domain. The area of the dusty air contains a semicylinder with a radius of 1 m. The size of the computational domain, initial parameters of the gas, parameters of the incoming shock, size of the semicylinder, and its location in the computational domain are the same as in the reflection and diffraction simulation presented in the previous section.

The main objective of this set of simulations is to study the effects of particle size and particle loading on the parameters

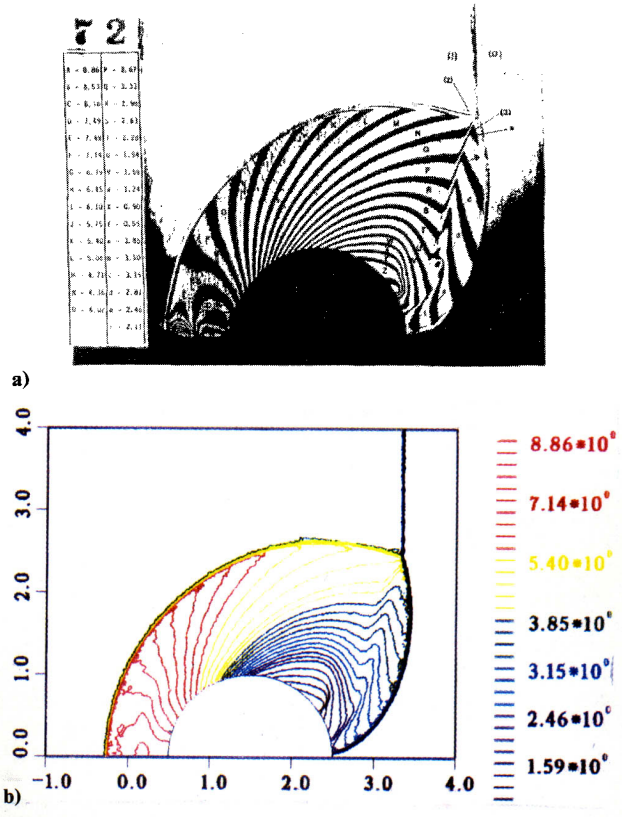

Fig. 5 Comparison for $M_s = 2.80$ gas-only flow: a) interferogram from experiment conducted by Kaca[22] and b) density contours from present calculation.

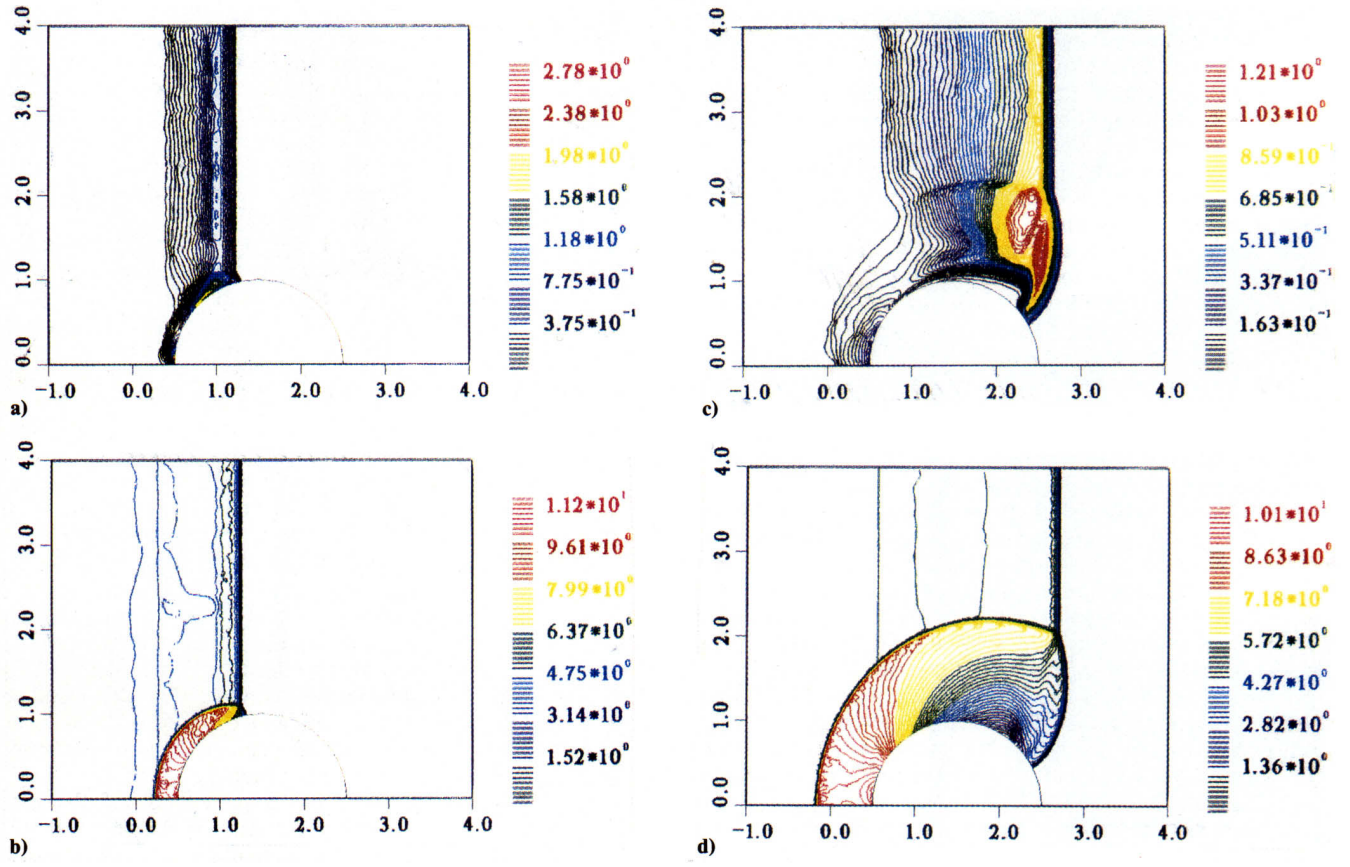

Fig. 6 Density contours for the case $M_s = 2.8$, $\rho_p = 0.25$ kg/m^3, and $r_p = 10$ μm at two different times: a) particle density at t_1; b) gas density at t_1; c) particle density at t_2; and d) gas density at t_2.

of the reflected and diffracted shock waves. It is also valuable to study the dynamics of particle media, since it is extremely difficult to observe these interactions experimentally in an optically thick dusty gas.

The first set of simulation results is shown for the case with dust parameters $r_p = 10$ μm and $\rho_p = 0.25$ kg/m^3. The gas parameters and the parameters of the incoming shock wave are the same as in the pure-gas case presented above. In Figs. 6a and 6b, particle-density contours and gas-density contours are shown at the stage when the incident shock wave has reached the top of the semicylinder. At this stage, the largest difference of velocity and temperature between the two phases exists and the nonequilibrium between the two phases causes extensive heat and momentum exchange between particles and the gas. The presence of the particles causes a widening of the shock that is more noticeable for the incident shock. Also, an additional contour line is observed at the dusty-gas/pure-gas interface. Comparing gas density for pure-gas flowfield shown in Fig. 4b and the dusty gas density of Fig. 6b, we see that Mach stem and contact discontinuity resulting from Mach reflection are smeared in the dusty gas flow due to the presence of the particle. The particle-density contours depict significant piling up of the dust particles at the leading-edge stagnation point of the cylinder.

In Figs. 6c and 6d, the particle-density and gas-density contours are shown at the stage where significant diffraction has taken place and the shock front is approaching the trailing edge of the cylinder. Further widening of the shock and some smearing of the slip line that originates at the triple point is evident. The particle-density contours reveal that the particles were swept by the gas flow to the area of triple point and slip line for the gas flow, leaving a small amount of particles at the leading edge. We should note that this behavior is specific for our problem, where at $t = 0$, the dusty gas area was located at $x = 0$ and there is no influx of the dust from the left boundary.

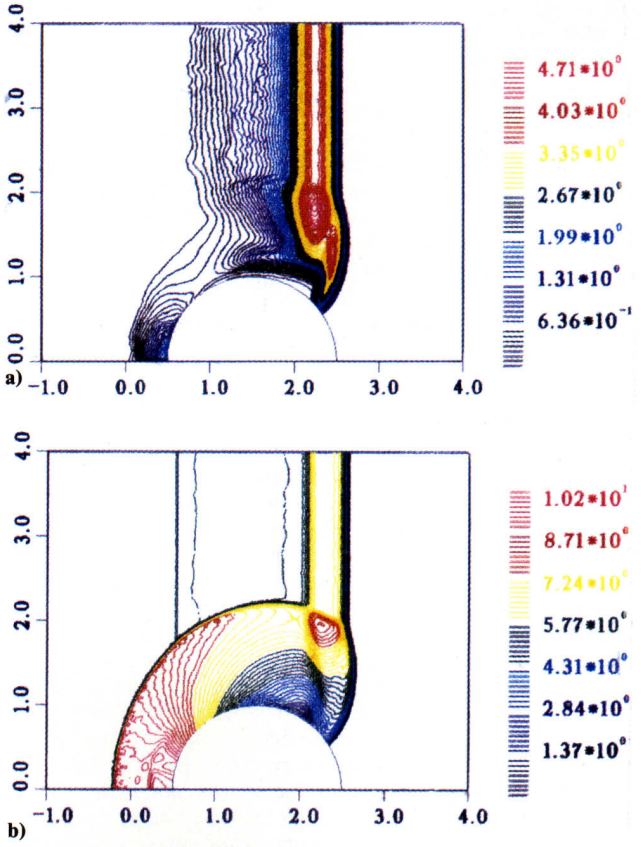

Fig. 7 Density contours for the case $M_s = 2.8$, $\rho_p = 0.76$ kg/m^3, and $r_p = 10$ μm: a) particle density and b) gas density.

Also in Fig. 6c, we note that the particles reach a distinct local maxima at the distance about 25 cm behind the incident shock front. At this maxima the particle density is 0.86 kg/m^3, which is more than three times the initial particle density. The particle density reaches a maximum value at the location of the gas slip line. We observe a significant accumulation of the particles that have been moved along the slip line by the shear flow. The larger concentration of particles in the vicinity of triple point is, in fact, the remainder of the particles that were swept up with the flow. It is also interesting to observe that an essentially particle-free zone is formed due to the effects of particles slipping over the top of the cylinder and the rarefaction wave behind the cylinder.

To study the influence of particle loading on the dynamics of reflection and diffraction, we have simulated the case with a dust density of $\rho_p = 0.76$, and with $r_p = 10$ μm. The results for this simulation are shown in Figs. 7a and 7b in the form of particle- and gas-density contour plots. In Fig. 7a, the particle-density contours are shown at the diffraction phase. Here we can observe two local maxima for particles accumulated in the regions along the slip line characteristic for the shock diffraction process. It should be noted here that in our problem the conditions behind the incident shock wave and its structure are in constant flux. At higher loading, dust will have a profound effect on the gasdynamics of reflection and diffraction. Figure 7b shows gas-density contours for the reflection stage corresponding to the particle-density contours shown in Fig. 7a. We observe from Fig. 7b that the incident shock wave is significantly smeared and the triple point cannot be clearly identified. Because of the widening of the incident shock, the area where the reflected and incident shock join is spread over a 50-cm distance. From Fig. 7a, we see that the high-density particle region is spread wider than in the previous case, and the particle density reaches its maximum at about 25 cm behind the front. There is a visible maximum in gas density in the area where the reflected shock is interacting with the area of maximum particle density behind the incident shock. A part of the reflected shock front that is moving to the left side of the computational domain is not affected by the dust since it is propagating into an area with little dust concentration. The parameters and structure of this part of the front remain basically the same as in the case of pure gas flow.

To examine the effect of particle size on the reflection-diffraction process, we simulated a case where the particle loading and gas-flow conditions are the same as in the previous case with particle density $\rho_p = 0.76$. However, the particle size is $r_p = 50$ μm. In Figs. 8a and 8b, results for this simulation are illustrated by particle-density and gas-density contours correspondingly. The particle contour plots depict a significantly wider particle relaxation zone than in the previous case. The longer relaxation zone is caused by the larger inertia of larger particles. The maximum particle density of 2.64 kg/m^3 is reached 50 cm behind the incident shock front. This value is significantly lower than 4.01 kg/m^3 reached behind the shock in calculation with 10-μm particles. Larger particles skip above the apex of the cylinder creating a void where particle density is very small. Also, because of larger particle size, the maxima of particle concentration that has been created by a slip surface of the reflected Mach stem is indistinct. The main reason for this is that the particles do not follow the gas flow as closely as they did in the previous case due to the inertia of large particles. The maximum particle density is reached here at the slip line behind the Mach stem.

Comparing gas density of Fig. 8b to the previous case shown in Fig. 7b, we observe that the slip line behind the curved Mach stem becomes less distinguishable in Fig. 7b. This result is expected, since at fixed particle loading, smaller particles have a larger surface/volume ratio and the larger surface/volume ratio increases momentum and heat exchange between the two phases.

One general comment regarding all three cases presented above: because of the heat and momentum exchange between the two phases, the shock is decaying as it traverses the cylinder. Ultimately, it will reach a new equilibrium state as suggested by Fig. 2. It should be noted that the shock considered in the previous three cases is still in the process of transition in the gas-particle mixture.

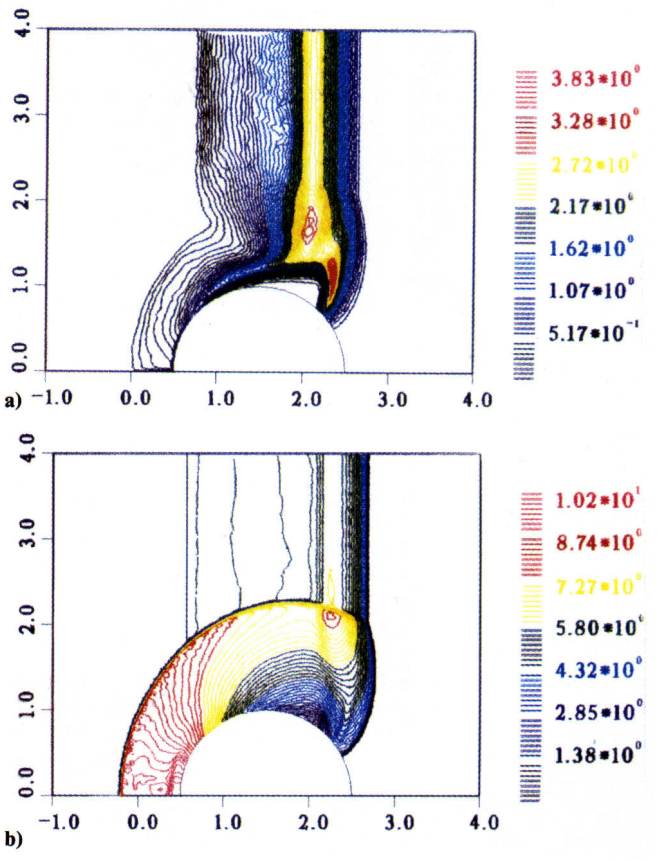

Fig. 8 Density contours for the case $M_s = 2.8$, $\rho_p = 0.76$ kg/m^3, and $r_p = 50$ μm: a) particle density and b) gas density.

IV. Conclusions

In this paper, a numerical study for a two-phase compressible flow is performed for the reflection and diffraction of a shock wave propagating over a semicircular cylinder in a dusty gas. The following conclusions can be made:

1) The validation study for a one-dimensional shock wave propagating in a dusty gas shows a good agreement between the prediction of our model and the results of the experiment.

2) For a two-dimensional gas-only flow, numerical results agree well with existing experimental data qualitatively and quantitatively, indicating that the gas phase is accurately simulated by the adaptive grid technique.

3) Particles in the gas can have a profound effect on the shock-wave reflection and diffraction pattern, which is a function of particle size and loading. The lesser the particle loading, the less the influence of particle on the flowfield.

4) In the three simulation cases, there is a particle accumulation behind the "back shoulder" of the semicircular cylinder due to the effect of particle inertia and gas rarefaction wave.

5) For different particle size at fixed particle loading, the larger particle will have a longer relaxation zone and less accumulation at "back shoulder" and behind incident shock. The gas-density contours show a less-distinguishable slip line in the small-particle case than in the large-particle case.

Acknowledgments

The work reported here was partially supported by the Defense Advanced Research Projects Agency and the Air Force Office of Scientific Research under Contract F49620-89-C-0087. The authors would like to thank J. Crowley and A. Nachman for their interest in this project.

References

[1]Marble, F., "Dynamics of Dusty Gases," *Annual Review of Fluid Mechanics,* Vol. 2, 1970, pp. 369–377.

[2]Rudinger, G., "Some Properties of Shock Relaxation in Gas Flows Carrying Small Particles," *Physics of Fluids,* Vol. 7, May 1964, pp. 658–663.

[3]Soo, S. L., *Particulates and Continuum,* Hemisphere Publishing Corp., New York, 1989, pp. 266–324.

[4]Crowe, C. T., "Review-Numerical Models for Dilute Gas Particle Flow," *Journal of Fluids Engineering,* Vol. 104, Sept. 1982, pp. 297–303.

[5]Hwang, C. J., and Chang, G. C., "Numerical Study of Gas-Particle Flow in a Solid Rocket Nozzle," *AIAA Journal,* Vol. 26, No. 6, 1988, pp. 682–689.

[6]Chang, I-S., "Three-Dimensional, Two-Phase, Transonic, Canted Nozzle Flows," *AIAA Journal,* Vol. 28, No. 5, 1989, pp. 790–797.

[7]Miura, H., and Glass, I. I., "Oblique Shock Wave in a Dusty-Gas Flow Over a Wedge," *Proceedings of Royal Society of London A,* Vol. 408, 1986, pp. 61–68.

[8]Sommerfeld, M., "The Unsteadiness of Shock Waves Propagating through Gas-Particle Mixtures," *Experiments in Fluids,* Vol. 3, No. 2, 1985, pp. 197–206.

[9]Kim, S.-W., and Chang, K.-S., "Reflection of Shock Wave from a Compression Corner in a Particle-Laden Gas Region," *Shock Waves,* Vol. 1, No. 3, 1991, pp. 65–73.

[10]Sichel, M., Baek, S. W., Kauffman, C. W., Maker, B., Nicholls, J. A., and Wolanski, P., "The Shock-Wave Ignition of Dusts," *AIAA Journal,* Vol. 23, No. 9, 1985, pp. 1374–1380.

[11]Fan, B., and Sichel, M., "A Comprehensive Model for the Structure and Dust Detonations," *Twenty-Second Symposium (International) on Combustion,* The Combustion Institute, PA, 1988, pp. 1741–1750.

[12]Clift, R., Grace, J. R., and Weber, M. E., *Bubbles, Drops and Particles,* Academic Press, New York, 1978.

[13]Drake, R. M., Jr., "Discussions on G. C. Vliet and G. Leppert: Forced Convection Heat Transfer from an Isothermal Sphere to Water," *Journal of Heat Transfer,* Vol. 83, No. 2, 1961, pp. 170–179.

[14]Eidelman, S., Colella, P., and Shreeve, R. P., "Application of the Godunov Method and Its Second Order Extension to Cascade Flow Modelling," *AIAA Journal,* Vol. 22, No. 11, 1984, pp. 1609–1615.

[15]Colella, P., "A Direct Eulerian MUSCL Scheme for Gas Dynamics," *SIAM Journal on Scientific and Statistical Computation,* Vol. 6, Jan. 1985, pp. 104–117.

[16]Colella, P., and Glaz, H. M., "Efficient Solution Algorithms for the Riemann Problem for Real Gases," *Journal of Computational Physics,* Vol. 59, No. 3, 1985, pp. 264–289.

[17]Peyret, R., and Taylor, T. D., *Computational Methods for Fluid Flow,* Springer-Verlag, New York, 1983, pp. 18–31.

[18]Ben-Dor, G., and Dewey, J. M., "The Mach Reflection Phenomenon: A Suggestion for an International Nomenclature," *AIAA Journal,* Vol. 23, No. 10, 1985, pp. 1650–1652.

[19]Hornung, H., "Regular and Mach Reflection of Shock Waves," *Annual Review of Fluid Mechanics,* Vol. 18, 1986, pp. 33–58.

[20]Yang, J. Y., Liu, Y., and Lomax, H., "Computation of Shock Wave Reflection by Circular Cylinder," *AIAA Journal,* Vol. 25, No. 5, 1987, pp. 683–689.

[21]Glass, I. I., Kaca, J., Zhang, D. L., Glaz, H. M., Bell, J. B., and Tangenstein, J., *Current Topics in Shock Waves, 17th International Symposium on Shock Tubes and Waves,* edited by Y. W. Kim, AIP Conf. Proceedings 208, American Institute of Physics, New York, 1990, pp. 246–251.

[22]Kaca, J., "An Interferometric Investigation of Diffraction of a Planar Shock Wave over a Semicircular Cylinder," *UTIAS Technical Note 269,* Inst. for Aerospace Studies, Univ. of Toronto, Canada, June 1988.